AJNR Am J Neuroradiol 20:713–716, April 1999

Technical Note

Diffusion Tensor MR Imaging and Comparative Histology of Glioma Engrafted in the Rat Spinal Cord

Ben A. Inglis, Debbie Neubauer, Lei Yang, Dan Plant, Thomas H. Mareci, and David Muir

Summary: MR imaging using contrast material derived from the diffusion of tissue water was tested for its ability to provide a nondestructive histologic analysis of tumor morphology. An apparent diffusion tensor MR image of a glioma engrafted within a rat spinal cord was generated in which fiber orientation in three dimensions was displayed in color. This imaging method clearly separated tumor from host white and gray matter and corresponded well with conventional histologic microscopy.

The translational free diffusion of water has been used extensively to provide a powerful endogenous contrast mechanism for MR imaging (1). The simplest approach uses a balanced pair of pulsed field gradients to obtain a diffusion-weighted image contrast (2–4). If desired, two or more diffusion-weighted images can be used for the calculation of an image of apparent diffusion coefficients, a measure of the apparent translational free diffusion rate of water. This method suffers from two limitations: only a unidirectional map of diffusion rate along the direction of the pulsed field gradient pair is produced, and the calculated diffusion coefficients vary with sample orientation in the gradient axis frame of reference. Recently, these limitations were overcome by the development of the apparent diffusion tensor (ADT) imaging method (5, 6). ADT imaging has now been used to obtain accurate diffusivity images of the normal brain (7–12) and spinal cord (13, 14).

In previous work, ADT imaging was applied to the histology of normal rat spinal cord (13). An idea presented by Nakada et al (15) and Matsuzawa et al (16) was extended to represent the trace of the ADT using a color scheme, a powerful way in which to characterize the complete ADT in a single image. The colored trace effectively allows three-dimensional fiber orientation to be displayed in a two-dimensional plane by providing, in effect, an MR ''stain'' (17) for relative fiber orientation. In our study, an ADT image of a glioma engrafted within a rat spinal cord was generated. The color trace image was compared with a standard histologic hematoxylin-eosin stain of sections cut from the same specimen to assess the ability of ADT imaging to differentiate host from tumor tissue.

This work used a very high field (14.1 T) vertical bore MR spectrometer in order to take advantage of the high inherent signal-to-noise ratio available. The present study was therefore limited to small-diameter tissue samples (eg, rat spinal cord or human nerve), yet it shows the potential of ADT imaging to provide a nondestructive histologic technique for assessing tumor location and extent. The high contrast between host tissue and tumor has considerable relevance to clinical oncology, in which diffusion-weighted MR and apparent diffusion coefficient imaging of tumors has already found utility (18–20). Given that ADT images were recently obtained from normal human brain using a standard clinical scanner (9–11), it seems reasonable to suggest that ADT imaging will become a powerful diagnostic technique for tumors as well. This is a promising technique because the source of contrast is endogenous.

Technique

The procedures for the engraftment of C6 tumors in the rat spinal cord were described in detail in a previous report (21). In brief, Sprague-Dawley rats (200 g) were deeply sedated and the thoracic spinal cord was exposed by laminectomy. The rat was mounted on a rodent spinal unit (Kopf Instruments, Tujunga, CA) and a suspension of rat C6 glioma cells (20,000/1.1 mL) was stereotactically injected at a depth of 1 mm. At 14 days after glioma cell implantation, the rats were given a heavy dose of sodium pentobarbital and killed by transcardiac perfusion with Ringer's vascular rinse followed by 4% paraformaldehyde in 0.1 M phosphate buffer (pH 7.2). The spinal cord was removed, and a 2.5-cm segment of cord surrounding the engraftment site was placed in a 5-mm-diameter glass tube filled with fixative. All surgical procedures met institutional Animal Care and Use Committee approval.

MR images were acquired at 14.1 T using a Varian Unity 600 imaging spectrometer (54 mm vertical bore) equipped with a gradient probe capable of 600 mT/m along *x* and *y* and 720 mT/m along *z*. All images were obtained using a spin-echo sequence with the read-refocus and phase-encoding gradients occurring in the first TE/2 period. For diffusion weighting, a

Received December 1, 1997; accepted after revision September 21, 1998.

Supported by grants from the National Institutes of Health (R01 NS29362 and P01 NS35702) (T.H.M.) and STOP! Children's Cancer, Inc (D.M.).

From Departments of Neuroscience (B.A.I.), Pediatrics (Neurology Division) (D.N., D.M.), Physics (L.Y.), and Biochemistry and Molecular Biology (T.H.M.), University of Florida, Gainesville; and the Center for Structural Biology, University of Florida Brain Institute (D.P.).

Address reprint requests to Ben A. Inglis, PhD, Center for Structural Biology, Box 100245, Health Science Center, University of Florida, Gainesville, FL 32610.

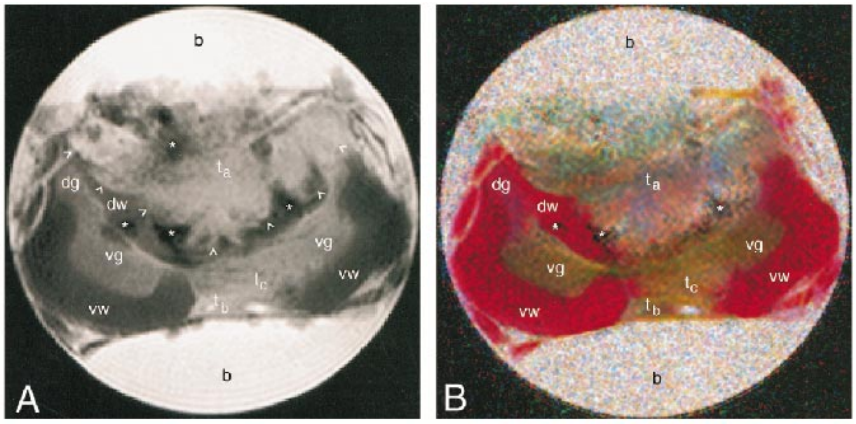

FIG 1. MR images of a glioma engrafted within rat cervical spinal cord (*b,* buffer; *dg,* dorsal gray matter; *dw,* dorsal white matter; *ta,* main tumor mass; *tb,* tumor located in the meninges; *tc,* tumor infiltrating to the ventral side; *vg,* ventral gray matter; *vw,* ventral white matter; *arrowheads,* main tumor border; *asterisks,* blood cells).

A, Conventional T2-weighted (3000/44) spin-echo image. Fixation tends to reduce the T2 of rat spinal cord, typical values being in the range 25 to 35 milliseconds. T1 is typically 180 to 220 milliseconds for fixed rat cord at 14.1 T.

B, Colored trace image from the same image plane as in *A,* formed from the ADT image. Diffusion directions are assigned as follows: blue, *x* (ventral-dorsal); green, *y* (left-right); red, *z* (perpendicular to plane).

separate pair of pulsed gradients were included in the sequence (2, 3). To obtain maximum diffusion sensitivity, the first diffusion gradient was applied immediately after the excitation RF pulse and the second just before acquisition. In all instances, the image field of view was 5 × 5 mm and the sample temperature was maintained at 20°C. Other acquisition parameters were as follows: 3000/44/4 (TR/TE/averages per phase-encode step); diffusion weighting gradient duration (δ), 10 milliseconds; diffusion weighting gradient pair separation (Δ), 26 milliseconds; and data matrix, 128 × 128. The in-plane resolution was 39 μm and the section thickness was 750 μm.

The tensor mapping procedure was adapted (13) from that described by Basser et al (5, 6). With the image plane fixed, diffusion-weighted images were acquired with diffusion weighting gradients aligned along the directions *x, y, z, x = z, y = z, x = y, and x = y = z.* In each gradient direction, a separate series of images was acquired with diffusion gradient amplitudes of 30, 90, 150, 210, and 270 mT/m, giving 35 separate image acquisitions overall. One further image was acquired without diffusion weighting gradients and was used to normalize the signal intensity of all diffusion-weighted images before calculation of the ADT. The overall measurement time was 15 hours.

The signal intensity in a diffusion-weighted image is related to the diffusion gradient strength through the b value. For each separate image acquisition a new matrix of b values was determined, taking into account all imaging and diffusion gradient auto- and cross-terms (22), except the phase-encoding gradient, which was considered to be 0 (ie, its central value) for simplicity. Trapezoidal gradient shapes were assumed and b matrices were found numerically using Mathematica (Wolfram Research, Inc, Champaign, Ill). At the largest diffusion weighting gradient of 270 mT/m, maximum values of 11583, 13914, and 11970 s/mm^2 were obtained for b_{xx}, b_{yy}, and b_{zz}, respectively, for phase encoding along *x,* read-out along *y,* and section selection along *z.*

On a pixel-by-pixel basis, multivariate matrix linear regression was used to find the six unique elements of the diffusion tensor, D_{ij} ($i,j = x,y,z$) according to:

$$\ln(S/S_{Gd=0}) = -\Sigma_{ij} b_{ij} D_{ij} + \ln(S_0/S_{Gd=0})$$

where S is the diffusion gradient-dependent signal intensity, $S_{Gd=0}$ is the experimental signal intensity without diffusion gradients, and S_0 is the theoretical signal intensity in the absence of all gradients. Matrix algebra was accomplished using Viewit (23).

The dimensionality of the complete ADT image was reduced by forming a color trace image, as described previously (13). The gray-scale diagonal element images of the complete tensor were first converted to eight-bit monochromatic images, assigned blue, green, and red for D_{xx}, D_{yy}, and D_{zz}, respectively, and then summed to obtain a 24-bit colored trace image (Photo-Paint 5.0, Corel Corp, Ottawa, Canada).

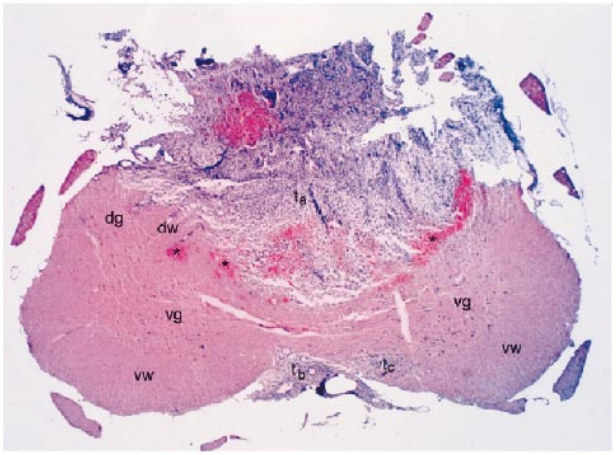

FIG 2. Hematoxylin-eosin–stained histologic section corresponding to the MR image plane in Figure 1. Labeled features are identified in the legend to Figure 1.

After completion of MR imaging, the spinal cord was removed from the tube holder and embedded in paraffin. Sections (7-μm thick) were stained with hematoxylin-eosin and then photographed by light microscopy using Kodak Royal Gold 25 print film.

Discussion

Accurate delineation of a CNS tumor boundary is one of the most critical parameters for effective therapy. Conventional MR methods rely on T1- and/or T2-weighted contrast using either the endogenous differences between host and tumor tissue or a contrast agent to highlight areas with a permeable blood-brain barrier. In either case, some level of a priori knowledge is required to select correctly the acquisition parameters. Diffusion tensor imaging does not rely on T1 and T2 signal weighting to provide contrast. Instead, the microstructure of different tissue types is reflected in the diffusion anisotropy of tissue water, and image con-

trast is obtained between regions with dissimilar diffusion anisotropies.

A conventional MR image of the spinal cord is shown in Figure 1A. Contrast arises primarily from T2-weighting (TE = 44) and the tumor mass appears bright. (Fixation tends to reduce the T2 of rat spinal cord, typical values being in the range of 25 to 35 milliseconds; T1 is typically 180 to 220 milliseconds for fixed rat cord at 14.1 T [Bossart EL, Silver X, Wirth ED, Mercer E, Inglis BA, Mareci TH, unpublished data].) The glioma occupies most of the dorsal half of the cord. Dark, almost black, areas are visible at the interface of the glioma and host tissue. It has been shown previously that such areas may result from cellular accumulation of paramagnetic species, such as iron-containing compounds (eg, blood cells), at the interface of tumor and host tissue (21). White matter tracts are hypointense relative to gray matter and glioma. Regions of gray matter and glioma are contrasted from white matter, but not well contrasted from each other. Owing to the complexity of the mass, it is difficult to assign tissue type or cellular detail for all regions in the image with complete certainty before comparison with microscopic analysis.

The color ADT image (Fig 1B) clearly differentiates gray from white matter and from glioma. Relative to the gradient axes, anisotropic diffusion along any given direction is assigned a unique color (13). A coloration indicates that there is a preferred direction for diffusion because of barriers to free diffusion; that is, semipermeable membranes and other features of the tissue microstructure that arise from cells, tracts, and so forth. A pixel having diffusion rates that are equal along *x*, *y* and *z* (isotropic diffusion) appears mottled and without a definite coloration. (In principle, if the fits of signal intensity versus b value were noiseless, then isotropic pixels would appear white.) This is the case for the buffer surrounding the cord. The red coloration of the white matter indicates fibers for which the predominant orientation is rostrocaudal; that is, water diffuses preferentially along the bundles of myelinated axons rather than across them. Note in particular the region of dorsal white matter to the left of the tumor that has been displaced ahead of the rapidly proliferating cells.

Green and blue coloration indicates fibers oriented predominantly in plane; for example, the gray matter horns. Tumor cells penetrating through to the ventral white matter can also be differentiated by their green/blue coloration. On the dorsal side, the translucent appearance of parts of the glioma is indicative of a low orientational anisotropy of this tissue; in other words, there is little organization of this tissue on the length scale of a pixel ($39 \times 39 \times 750$ μm).

The color ADT image correlates extremely well with conventional histology (Fig 2). All gross morphologic features seen in the color ADT trace image are confirmed by the hematoxylin-eosin–stained section. The section clearly shows the tumor mass and the tumor cells penetrating the ventral white matter. Normally appearing white and gray matter are discernible, as is the displaced region of dorsal funiculus to the left of the main tumor mass. Areas of bright red on the histologic section are indicative of blood cells. These regions correspond to dark regions on both the MR images and are consistent with a loss of MR signal caused by paramagnetic species.

Conclusion

There is excellent agreement between color ADT MR imaging and conventional histologic microscopy. The ADT method yields image contrast that reflects tissue microstructure and that is inherently three-dimensional in character. It delineates gray from white matter and from glioma unambiguously by virtue of their different cellular structures. The nature of this contrast is inherently different from conventional endogenous (T1- or T2-weighted) MR contrast and may prove to be more sensitive for certain tumor types. We expect that ADT imaging will find widespread application in clinical oncology as more clinical MR scanners are outfitted with ADT-capable software. Although this study used b values an order of magnitude larger than are available on most clinical scanners, large b values are not necessary in the ADT method. Complete ADT images have been obtained from normal human brain (9–11) by making only slight modifications to the experimental protocol described here.

References

1. LeBihan D. ***Diffusion and Perfusion Magnetic Resonance Imaging Applications to Functional MRI.*** New York: Raven Press; 1995
2. LeBihan D, Breton E. **Imagerie de diffusion in-vivo par resonance magnetique nucleaire.** *Cr Acad Sci (Paris)* 1985;301: 1109–1112
3. Taylor DG, Bushell MC. **The spatial mapping of translational diffusion coefficients by the NMR imaging technique.** *Phys Med Biol* 1985;30:345–349
4. Merboldt KD, Hanicke W, Frahm J. **Self-diffusion NMR imaging using stimulated echoes.** *J Magn Reson* 1985;64:479–486
5. Basser PJ, Mattiello J, LeBihan D. **MR diffusion tensor spectroscopy and imaging.** *Biophys J* 1994;66:259–267
6. Basser PJ, Mattiello J, LeBihan D. **Estimation of the effective self-diffusion tensor from the NMR spin echo.** *J Magn Reson* 1994**[**03;247–254
7. van Gelderen P, de Vleeschouwer MHM, DesPres D, Pekar J, van Zijl PCM, Moonen CTW. **Water diffusion and acute stroke.** *Magn Reson Med* 1994;31:154
8. Mori S, van Zijl PCM. **Diffusion weighting by the trace of the diffusion tensor within a single scan.** *Magn Reson Med* 1995; 33:41–52
9. Pierpaoli C, Basser PJ. **Toward a quantitative assessment of diffusion anisotropy.** *Magn Reson Med* 1996;36:893–906
10. Pierpaoli C, Jezzard P, Passer PJ, Barnett A, Di Chiro G. **Diffusion tensor MR imaging of the human brain.** *Radiology* 1996;201: 637–648
11. Basser PJ, Pierpaoli C. **Microstructural and physiological features of tissues elucidated by quantitative diffusion tensor MRI.** *J Magn Reson* 1996**[**11:209–219
12. Lythgoe MF, Busza AL, Calamante F, et al. **Effects of diffusion anisotropy on lesion delineation in a rat model of cerebral ischemia.** *Magn Reson Med* 1997;38:662–668

13. Inglis BA, Yang L, Wirth ED, Plant D, Mareci TH. **Diffusion anisotropy in excised normal rat spinal cord measured by NMR microscopy.** *Magn Reson Imaging* 1997;15:441–450
14. Gulani V, Iwamoto GA, Jiang H, Shimony JS, Webb AG, Lauterbur PC. **A multiple echo pulse sequence for diffusion tensor imaging and its application in excised rat spinal cords.** *Magn Reson Med* 1997;38:868–873
15. Nakada T, Matsuzawa H, Kwee IL. **Magnetic resonance axonography of the rat spinal cord.** *Neuroreport* 1994;5:2053–2056
16. Matsuzawa H, Kwee IL, Nakada T. **Magnetic resonance axonography of the rat spinal cord: postmortem effects.** *J Neurosurg* 1995;83:1023–1028
17. Johnson GA, Beneviste H, Black RD, Hedlund LW, Maronprot RR, Smith BR. **Histology by magnetic resonance microscopy.** *Magn Reson Q* 1993;9:1–30
18. Ebisu T, Tanaka C, Umeda M, et al. **Discrimination of brain abscess from necrotic or cystic tumors by diffusion-weighted echo planar imaging.** *Magn Reson Imaging* 1996;14:1113–1116
19. Krabbe K, Gideon P, Wagn P, Hansen U, Thomsen C, Madsen F. **MR diffusion imaging of human intracranial tumors.** *Neuroradiology* 1997;39:483–489
20. Maier CF, Paran Y, Bendel P, Rutt BK, Degani H. **Quantitative diffusion imaging in implanted human breast tumors.** *Magn Reson Med* 1997;37:576–581
21. Muir D, Johnson J, Rojiani M, Inglis BA, Rojiani A, Maria BL. **Assessment of laminin-mediated glioma invasion in vitro and by glioma tumors engrafted within rat spinal cord.** *J Neuro Oncol* 1996;30:199–211
22. Mattiello J, Basser PJ, LeBihan D. **Analytical expressions for the b matrix in NMR diffusion imaging and spectroscopy.** *J Magn Reson* 1994T08;131–141
23. Potter CS, Moran PJ. **Viewit: a software system for multi-dimensional biomedical image processing, analysis and visualization.** *Proceedings of the 3rd SPIE Conference on Biomedical Image Processing and 3-D Microscopy.* 1992;1660:767–773